

DRIV-EX: Counterfactual Explanations for Driving LLMs

Amaia Cardiel^{1,2}, Eloi Zablocki², Elias Ramzi², Eric Gaussier¹

¹ Aptikal, Université Grenoble Alpes, Grenoble, France

² Valeo.ai, Paris, France

Abstract

Large language models (LLMs) are increasingly used as reasoning engines in autonomous driving, yet their decision-making remains opaque. We propose to study their decision process through counterfactual explanations, which identify the minimal semantic changes to a scene description required to alter a driving plan. We introduce DRIV-EX, a method that leverages gradient-based optimization on continuous embeddings to identify the input shifts required to flip the model’s decision. Crucially, to avoid the incoherent text typical of unconstrained continuous optimization, DRIV-EX uses these optimized embeddings solely as a *semantic guide*: they are used to bias a controlled decoding process that re-generates the original scene description. This approach effectively steers the generation toward the counterfactual target while guaranteeing the linguistic fluency, domain validity, and proximity to the original input essential for interpretability. Evaluated using the LC-LLM planner on the textual highD dataset, DRIV-EX generates valid, fluent counterfactuals more reliably than existing baselines. It successfully exposes latent biases and provides concrete insights to improve the robustness of LLM-based driving agents. The code will be released.

1 Introduction

End-to-end Autonomous Driving (AD) increasingly relies on Large Language Models (LLMs) and Vision-Language Models (VLMs). Thanks to large-scale pre-training, these models can integrate user instructions and sensor inputs to directly generate driving decisions (Rowe et al., 2025; Hwang et al., 2025; Renz et al., 2024, 2025; NVIDIA, 2025). Unlike traditional neural planners that operate as black boxes, LLM-based systems provide natural language explanations, e.g., with Chain-of-Thought (CoT) (Renz et al., 2025; Peng et al., 2024; NVIDIA, 2025). However, reliance on these

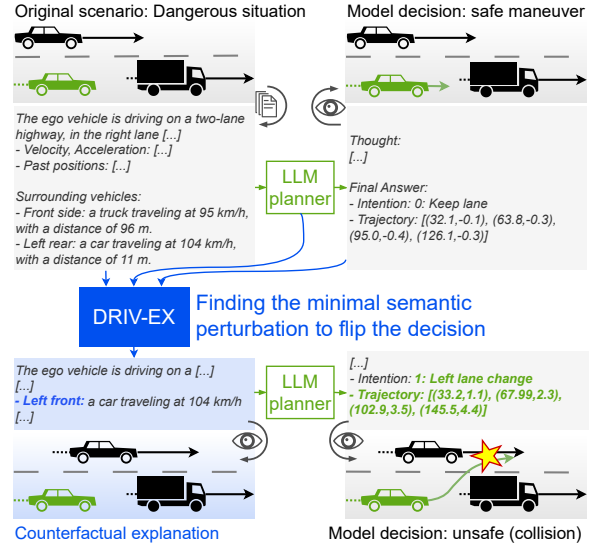


Figure 1: **Overview of DRIV-EX counterfactual generation.** The LLM acts as the planner for the ego vehicle (in green). Given an initial driving scenario where the planner behaves safely (top row), our method automatically identifies a minimal semantic perturbation to the scene description (such as slightly altering the position or speed of surrounding vehicles) that forces the model into a dangerous failure mode (bottom row). By uncovering these decision boundaries, DRIV-EX exposes latent biases and evaluates the robustness of driving agents against critical edge cases.

explanations is risky: recent work shows that CoT reasoning is often an unfaithful post-hoc rationalization that does not reflect the features actually driving the prediction (Turpin et al., 2023). Yet, Barez et al. (2025) report that 63% of recent autonomous systems papers treat CoT as an *interpretability* method. In safety-critical domains, such unfaithful explanations can mask the true causes of dangerous behaviors, creating a strong need for methods that directly identify the input factors responsible for catastrophic decisions.

Counterfactual explanations offer a grounded alternative to narrative-based insights. By identifying the minimal change to an input that would lead the

model to make a different decision, counterfactuals explicitly isolate the causal features of a behavior. In the context of LLM-based driving, this involves finding the smallest modification to a scene description that turns a safe maneuver into a collision (or vice versa). As illustrated in Fig. 1, this provides a concrete mechanism to audit decision boundaries and expose latent safety risks.

Technically, generating these textual counterfactuals requires solving a difficult discrete optimization problem: finding a sequence of tokens that is semantically close to the original description yet validly flips the driving decision. This presents a dilemma between two standard approaches. *Gradient-based methods* (often used in ‘soft’ prompt optimization) relax discrete text into continuous embeddings to efficiently search for decision boundaries, but they generally fail to recover coherent text when projected back to the discrete vocabulary (Kumar et al., 2022; Wen et al., 2023). Conversely, *discrete search methods* that rely on the model’s native autoregressive sampling ensure fluency but lack the gradient guidance needed to efficiently cross the decision boundary (Liu et al., 2023; Pynadath and Zhang, 2025). Lastly, satisfying the *minimality* constraint is particularly challenging: without robust regularization, optimization algorithms tend to drift far from the original input, hallucinating entirely new objects or contexts rather than isolating the subtle feature shifts that explain the model’s behavior.

In this work, we introduce DRIV-EX (DRIVing EXplanations), an algorithm designed to resolve this tension. Our key idea is to decouple the *search* for the counterfactual from its *generation*. DRIV-EX treats optimized continuous embeddings from gradient-based methods not as the final output, but as a *semantic guide* for a controlled decoding framework. Practically, our algorithm performs gradient-based updates on the unconstrained prompt embeddings to identify the direction required to flip the decision. Then, it uses these embeddings to bias an autoregressive re-generation of the input. This allows us to steer the fluent generation capabilities of the LLM toward the critical decision boundaries identified by the gradients, effectively combining the search power of continuous optimization with the coherence of autoregressive generation.

We evaluate DRIV-EX through quantitative experiments on LC-LLM (Peng et al., 2024), a recent driving LLM planner, using a textual transcription

of the highD dataset (Krajewski et al., 2018), a real-world highway driving benchmark. We show that DRIV-EX generates valid counterfactuals more reliably than existing baselines (Pynadath and Zhang, 2025; Wen et al., 2023). We further use DRIV-EX to reveal biases that push models toward unsafe decisions. Finally, we demonstrate that these insights can be used to mitigate such biases, improving the safety and robustness of driving LLM planners.

2 Related Work

Explainability methods for NLP models are commonly divided into local and global approaches (Zhao et al., 2024). Local methods explain individual predictions, typically via attribution techniques (Li et al., 2016; Wu et al., 2020; Mohebbi et al., 2021; Enguehard, 2023). Global approaches, including mechanistic interpretability, aim to uncover model-wide behaviors that generalize across inputs (Bricken et al., 2023; Conmy et al., 2023), but are less suited to explaining specific decisions.

Counterfactual explanations are a form of local interpretability, identifying minimal changes to an input that would alter a model’s prediction and thereby exposing causal decision factors (Wachter et al., 2017). In NLP, they have been studied for discriminative tasks such as sentiment analysis and toxicity detection (Wu et al., 2021; Nguyen et al., 2024). Typical approaches generate counterfactuals by substituting, masking, or infilling tokens while preserving fluency and meaning (Wu et al., 2021). Most NLP counterfactual methods follow a two-stage pipeline: (i) identifying influential input tokens, and (ii) editing these tokens to induce a label change (Ross et al., 2021; Fern and Pope, 2021; Treviso et al., 2023). For example, MiCE (Ross et al., 2021) selects tokens via gradient-based attribution and enforces minimality through constrained search, while CREST (Treviso et al., 2023) leverages sparse rationales to relax strict edit minimality. TIGTEC (Bhan et al., 2023) similarly performs sequential masked token replacement guided by local importance.

Despite operating in discrete text space, these methods are not directly applicable to our setting. They are designed for discriminative classifiers where the prediction is a direct mapping from a static input to a label. In contrast, LLM planners operate autoregressively, meaning the probability of a decision token depends heavily on the sequence of preceding tokens. This imposes a strictly harder

constraint: a valid counterfactual must not only flip the target decision but also preserve the high likelihood of the entire preceding generation trajectory.

Prompt optimization methods search for discrete or continuous input prompts that induce desired behaviors from pretrained language models. Soft prompt tuning introduces continuous embeddings optimized via gradients without updating model parameters (Lester et al., 2021; Li and Liang, 2021). Discrete approaches such as AutoPrompt (Shin et al., 2020) and PEZ (Wen et al., 2023) perform gradient-based updates in embedding space followed by projection to discrete tokens.

Related techniques have been explored extensively in adversarial prompting, jailbreak attacks, and red teaming, where the goal is to elicit unsafe or restricted behaviors from fixed LLMs (Wallace et al., 2019; Guo et al., 2024; Zou et al., 2023; Mo et al., 2024). These methods typically prioritize objective satisfaction over semantic fidelity, often producing prompts that are unnatural or out of distribution.

Our work shares the underlying optimization structure of these approaches: searching over token sequences to satisfy a target objective. However, it differs in motivation and constraints. Rather than inducing arbitrary or adversarial behaviors, we seek minimal, instance-specific edits that preserve semantic plausibility while flipping a concrete decision. This places stronger constraints on fluency, proximity, and interpretability than most prompt optimization or attack-oriented methods enforce.

Controlled decoding methods steer pretrained autoregressive models at inference time so that generated sequences satisfy explicit constraints while remaining fluent (Scholak et al., 2021; Yang and Klein, 2021). Approaches include biased autoregressive sampling (Liu et al., 2023), reinforcement learning over decoding policies (Mudgal et al., 2024), and gradient-based sampling methods combining multiple objectives (Qin et al., 2022; Kumar et al., 2022; Pynadath and Zhang, 2025). Several methods explicitly operate in discrete token space using local edits or MCMC-style proposals. For example, MuCoLa (Kumar et al., 2022) performs constrained editing via MCMC to balance constraint satisfaction and likelihood, while DAB (Pynadath and Zhang, 2025) combines discrete Langevin proposals with biased autoregressive generation to improve exploration near constraint boundaries.

While controlled decoding is closely related to

our approach, key differences remain. Controlled decoding is typically framed as a generation problem without a reference input, targeting global attributes such as sentiment or topic. In contrast, our task is explicitly counterfactual: we operate relative to a specific reference prompt and enforce semantic proximity to it. This shifts the objective from general constraint satisfaction to fine-grained, local edits that expose decision boundaries.

3 Method: DRIV-EX

3.1 Problem and method overview

Formalization. Let \mathcal{M} be an autoregressive language model with vocabulary V . Given an original input sequence $\mathbf{x}^o = (x_1^o, \dots, x_m^o) \in V^m$, the model produces the sequence $\mathbf{y}^o = (y_1^o, \dots, y_n^o) = \mathcal{M}(\mathbf{x}^o)$. We focus on a particular decision made during generation, formalized as the token emitted at the semantic decoding step T (e.g., the first token encoding a planning decision in a structured output). Importantly, T refers to a semantic position rather than a fixed index and may depend on the generated prefix. As observed in prior work on LLM steering and jailbreaks, influencing the first critical decision token is often sufficient to redirect the entire subsequent generation (Wei et al., 2023; Carlini et al., 2023; Zou et al., 2023) since autoregressive dynamics strongly bias the continuation. This motivates focusing the counterfactual search on enforcing the constraint at step T . Empirical evidence for this phenomenon is given in App. A.

We seek a counterfactual explanation \mathbf{x} that induces a target decision y_T^* at step T , while remaining a minimal and plausible modification of \mathbf{x}^o . This yields competing objectives: (i) enforcing the desired *decision* at step T , (ii) preserving *fluency*, and (iii) semantic *proximity* to the initial input. We express this as a constrained optimization problem:

$$\begin{aligned} \arg \min_{\mathbf{x} \in V^m} \quad & c(\mathbf{x}^o, \mathbf{x}) \\ \text{s.t.} \quad & y_T^* = \arg \max_{z \in V} P_{\mathcal{M}}(z \mid \mathbf{y}_{<T}, \mathbf{x}), \end{aligned} \quad (1)$$

where $c(\mathbf{x}^o, \mathbf{x})$ is a cost function capturing proximity and fluency.

High-level method idea. Directly optimizing the counterfactual objective in Eq. 1 is challenging because the input \mathbf{x} lies in a discrete space and the autoregressive decoding process of LLMs is non-differentiable. Naively relaxing the input to a continuous space enables gradient-based prompt

Algorithm 1: DRIV-EX pseudo-code

Input: Original input $\mathbf{x}^o = (x_1^o, \dots, x_m^o)$;
target token y_T^* at step T ; model \mathcal{M}

Output: Counterfactual explanation \mathbf{x}^{cf}

Initialize soft embeddings \mathbf{e} using \mathbf{x}^o ;

for $n = 1$ **to** N **do**

▷ *Projection and forward pass:*

Project \mathbf{e} to get \mathbf{x} ; // Eq. 2

Compute decision loss \mathcal{L}_{dec} ; // Eq. 3

▷ *Backward (straight-through update):*

Compute gradient $\nabla_{\mathbf{x}} \mathcal{L}_{\text{dec}}$;

Update soft embeddings \mathbf{e} ; // Eq. 4

▷ *Regularized autoregressive decoding:*

Compute biases \mathcal{B} and \mathcal{B}' from \mathbf{e} and

\mathbf{x}^o ; // Eq. 5–6

Decode candidate x with biased
decoding; // Eq. 7

return \mathbf{x}^{cf} ; // Best candidate x

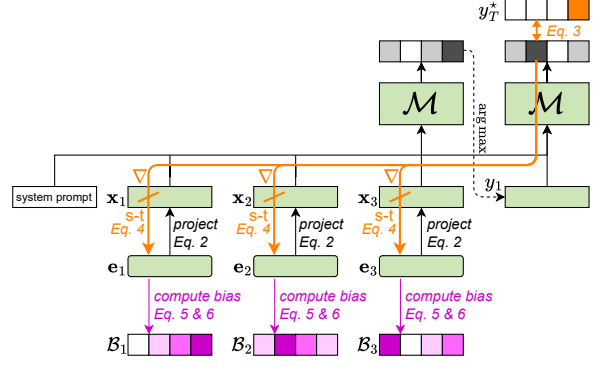


Figure 2: **Forward and backward passes, and bias computation.** In the forward pass (black), the continuous soft embeddings \mathbf{e} are projected onto their nearest discrete neighbors in the vocabulary to obtain tokens \mathbf{x} , following Eq. 2. These tokens are then processed by the model \mathcal{M} to compute the probability $P_{\mathcal{M}}(y_T^* | \mathbf{y}_{<T}, \mathbf{x})$. In the backward pass (orange), the model calculates the loss relative to the desired target token y_T^* (Eq. 3). Gradients (∇) are backpropagated from the target decision and, using a straight-through (s-t) estimator, bypass the discrete projection to update the continuous embeddings \mathbf{e} (Eq. 4). Finally, the updated embeddings are converted into vocabulary bias terms (\mathcal{B} , in pink) to guide subsequent regularization (following Eq. 5–6).

optimization with straight-through gradients (Shin et al., 2020; Wen et al., 2023), but discretizing the resulting embeddings often leads to incoherent or out of distribution text, violating the plausibility requirement.

To address this, we decouple the *search* for the counterfactual from its *generation*. We utilize the optimized continuous embeddings not as final outputs but as a *semantic guide* within a controlled decoding framework (Liu et al., 2023; Pynadath and Zhang, 2025). Specifically, we perform gradient-based updates on the embeddings to identify the direction required to flip the decision. We then use these embeddings to bias an autoregressive re-generation of the input, steering the sampling toward the identified decision boundary and the original text while strictly enforcing fluency. The complete procedure is summarized in algorithm 1.

3.2 Discrete counterfactual optimization via straight-through embeddings

Continuous relaxation. We associate each input token with a continuous embedding and maintain a sequence of soft embeddings $\mathbf{e} = (\mathbf{e}_1, \dots, \mathbf{e}_m) \in \mathbb{R}^{m \times d}$, initialized from the embeddings of the original input \mathbf{x}^o . At each iteration, the current soft embeddings are projected onto the nearest vocabulary embeddings using cosine similarity:

$$\mathbf{x}_i = \text{Proj}_E(\mathbf{e}_i) := \arg \max_{\mathbf{v} \in E} \frac{\mathbf{e}_i \cdot \mathbf{v}}{\|\mathbf{e}_i\| \|\mathbf{v}\|}, \quad (2)$$

yielding a discrete token sequence \mathbf{x} compatible with the LLM’s vocabulary.

Decision-driven gradient update. The projected sequence \mathbf{x} is fed to the model \mathcal{M} to evaluate the decision objective at step T :

$$\mathcal{L}_{\text{dec}}(\mathbf{x}) = -\log P_{\mathcal{M}}(y_T^* | \mathbf{y}_{<T}, \mathbf{x}), \quad (3)$$

and compute gradients with respect to the projected embeddings linked to \mathbf{x} . Using a straight-through estimator (Bengio et al., 2013), these gradients are applied to the continuous embeddings \mathbf{e} , which are updated via Adam (Kingma and Ba, 2015):

$$\mathbf{e} \leftarrow \text{Adam}(\mathbf{e}, \nabla_{\mathbf{x}} \mathcal{L}_{\text{dec}}, \eta). \quad (4)$$

This process is illustrated in Fig. 2.

This project-forward-backward-update loop constitutes the core optimization algorithm and is repeated a predefined number of N iterations.

3.3 Projection-based regularization and evaluation

While the gradient-based updates in Sec. 3.2 effectively inject the decision-change signal into the continuous embeddings \mathbf{e} , directly projecting these embeddings onto the vocabulary often yields incoherent sequences that fail to satisfy the plausibility

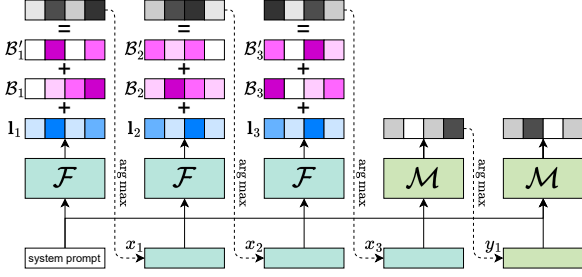


Figure 3: **Regularized autoregressive decoding.** During the regularization phase, the vocabulary bias terms \mathcal{B} and \mathcal{B}' (derived from optimized embeddings and \mathbf{x}^o) are added to the logits \mathbf{l} of a fluency model \mathcal{F} . This combined signal biases the auto-regressive decoding, following Eq. 7, to generate a new candidate sequence (x_1, x_2, x_3) that incorporates the decision-change signal while maintaining fluency and input proximity.

constraint. To bridge this gap, we employ a regularized autoregressive decoding strategy (Liu et al., 2023; Pynadath and Zhang, 2025) where the optimized embeddings serve as a *semantic guide* to steer a dedicated fluency model \mathcal{F} . We instantiate \mathcal{F} as the pre-trained base model of \mathcal{M} (i.e., without instruction-tuning adapters) to guarantee a shared vocabulary and tokenization, enabling us to directly bias its logits using distances computed in the common embedding space.

Fluency regularization with biased autoregressive decoding. For each position i , we compute a distance vector $\tilde{\mathbf{b}}_i \in \mathbb{R}^{|\mathcal{V}|}$ measuring how far each vocabulary token v is from the projected token $\text{Proj}_E(\mathbf{e}_i)$ in embedding space:

$$b_{i,v} = \|\mathbf{v} - \text{Proj}_E(\mathbf{e}_i)\|_2^2. \quad (5)$$

To match the scale of the model logits $\mathbf{l}_i = \text{logits}_{\mathcal{F}}(\cdot | x_{<i})$, we compute a normalization factor $r_i = \|\mathbf{l}_i\|_2 / \|\mathbf{b}_i\|_2$ as in Pynadath and Zhang (2025). The bias applied to each token v is then

$$\mathcal{B}_{i,v} = -w \cdot r_i \cdot b_{i,v}, \quad (6)$$

where w controls the strength of the bias.

The bias is added to the logits of the fluency model \mathcal{F} during greedy decoding, encouraging generations that are close to the optimized embeddings while preserving fluency. Concretely, as illustrated in Fig. 3, the next token is chosen with: $x_i = \arg \max_{v \in \mathcal{V}} (l_{i,v} + \mathcal{B}_{i,v})$.

The resulting decoded sequence provides a concrete counterfactual candidate that can be evaluated against the objective in Eq. 1. Importantly, this regularization does not define a separate optimization

step but serves to monitor and enforce plausibility throughout the optimization trajectory.

Input proximity regularization. We propose three complementary approaches to ensure semantic proximity to \mathbf{x}^o . First, ‘**Proj**’ implies to limit embedding projections (Eq. 2) to the subset of the top K nearest neighbors of \mathbf{x}^o (in cosine similarity). Second, ‘**Loss**’ adds $(1 - \frac{1}{m} \sum_{i=1}^m \cos \text{sim}(\mathbf{x}_i, \mathbf{x}_i^o))$ as a regularization term to the decision loss (Eq. 3), controlled by a weight λ . Finally, ‘**Bias**’ adds a second bias during autoregressive biasing (Eq. 7). Using \mathbf{x}_i^o instead of the current projected token $\text{Proj}_E(\mathbf{e}_i)$ in Eq. 5, we compute $\mathcal{B}'_{i,v}$ following Eq. (5)–(6), and the biased sampling becomes:

$$x_i = \arg \max_{v \in \mathcal{V}} (l_{i,v} + \mathcal{B}_{i,v} + \mathcal{B}'_{i,v}). \quad (7)$$

Best candidate selection. Upon completion of N iterations, we use a heuristic selection to derive the best counterfactual x from the pool of generated candidates. We prioritize candidates that successfully trigger the decision change; specifically, we define the set of valid candidates as those satisfying $y_T^* = \arg \max_{z \in \mathcal{V}} P_{\mathcal{M}}(z | \mathbf{y}_{<T}, x)$. If this set is non-empty, we return the candidate that maximizes semantic proximity to the original input \mathbf{x}^o , as the autoregressive decoding is already ensuring high fluency. Conversely, if no candidate triggers the decision change, we return the sequence that achieves the highest target probability $P_{\mathcal{M}}(y_T^* | \mathbf{y}_{<T}, x)$.

4 Experiments

We evaluate DRIV-EX on LC-LLM (Peng et al., 2024), a LoRA-finetuned planner (Hu et al., 2022), on the textual transcription of the highD dataset (Krajewski et al., 2018). This dataset maps traffic annotations to discrete Lane Change (LC) commands and trajectories.

4.1 Experimental Protocol

We focus on probing the brittleness of the model’s safety predictions. From the validation set, we select ‘*dangerous*’ scenarios, defined as those where the ground-truth trajectory implies a potential collision (impact within 4s at constant velocity). We further focus on scenarios where the model predicts a ‘*safe*’ maneuver. To assess robustness, we investigate whether minimal semantic perturbations to these scenes can force the model into a catastrophic failure. We set the target y_T^* to the ground-truth LC token, and employ DRIV-EX to flip the model’s

Method	LLM	Decision	Fluency		Similarity	Aggregation	
		y_T^* has top rank (%)	Min fluency ↑	Temp fit (%) ↑	BERT Score (%) ↑	Aggreg (%) ↑	Aggreg & col (%) ↑
DAB (Pynadath and Zhang, 2025)	Llama3	100.0	9e-4	99.3	93.5	33.3	14.7
	Mistral	91.8	6e-3	86.4	90.4	24.5	20.4
	Qwen2.5	98.9	2e-3	53.2	79.6	7.8	7.8
DAB †	Llama3	46.7	5e-3	100.0	98.1	41.3	30.7
	Mistral	40.8	3e-2	99.9	97.7	38.8	34.7
	Qwen2.5	26.7	7e-3	99.8	97.8	24.4	21.1
PEZ (Wen et al., 2023)	Llama3	97.3	2e-4	93.8	97.5	45.3	37.3
	Mistral	100.0	5e-4	93.0	97.5	42.9	36.7
	Qwen2.5	96.7	2e-3	86.2	92.9	23.3	17.8
PEZ †	Llama3	97.3	2e-4	95.4	97.8	49.3	37.3
	Mistral	98.0	3e-4	95.0	98.0	42.9	36.7
	Qwen2.5	94.4	3e-3	89.9	95.2	30.0	23.3
DRIV-EX (ours)	Llama3	64.0	1e-3	99.5	98.3	61.3	56.0
	Mistral	83.7	4e-3	98.5	97.8	69.4	61.2
	Qwen2.5	58.9	3e-3	96.4	96.6	34.4	<u>22.2</u>

Table 1: **Main counterfactual explanation results** on safety-critical textual highD subsets. We report metrics for steering LLMs from a safe decision to a collision. All methods use a comparable compute budget: $N = 15$ iterations for DAB/DRIV-EX, $N = 100$ –150 for PEZ. ‘†’ denotes task-adapted baselines (vs. off-the-shelf ones).

decision from ‘safe’ to ‘dangerous’. For all algorithms, optimization is restricted to tokens of variable words in the driving template (e.g., vehicle type, speed, position). These tokens are shown in Sec. C.2, Fig. 8 and subset statistics are given in Tab. 10. This setup allows us to (1) benchmark DRIV-EX against existing baselines (Sec. 4.2), (2) uncover dataset biases that trigger unsafe decisions (Sec. 4.3), and (3) demonstrate how these insights can mitigate bias and improve safety (Sec. 4.4).

4.2 Comparison with baselines and ablations

We compare DRIV-EX against DAB (Pynadath and Zhang, 2025), PEZ (Wen et al., 2023), and their task-adapted versions (†) across instructed versions of Llama3-8B (Dubey et al., 2024), Mistral-7B (Jiang et al., 2023), and Qwen2.5-7B (Yang et al., 2024). Implementation, baseline adaptation and hyperparameter search are detailed in App. D.

Evaluation Metrics. We track metrics that map to the counterfactual explanation constraints:

- **Decision (P@1):** Success if the target y_T^* is the top-ranked token at step T .

- **Similarity and Fluency: BERTScore** (Zhang et al., 2020) measures semantic proximity to the original input; **Template Fitness** verifies if the generated text adheres to the rigid template of the driving prompt; **Minimum Fluency** is the minimum

conditional token probability (cf Eq. 8 in Sec. B.1).

- **Aggregated Scores (Success Rate):** These are our primary metrics that we optimize. ‘Aggreg’ measures the number of counterfactual ‘Successes’. A counterfactual is a ‘Success’ if it satisfies three strict conditions: the decision is flipped (P@1), the template is valid (100% fitness), and semantic similarity is high (BERTScore ≥ 0.95). More details on metrics and thresholds in Sec. B.1. We also report ‘Aggreg & Col’, the subset of successes that lead to a collision. It quantifies the method’s ability to expose physically dangerous behaviors.

Quantitative results. Generating counterfactuals requires balancing decision flipping with similarity and fluency. As shown in Tab. 1, off-the-shelf DAB achieves high P@1 (100% for Llama3) but fails on similarity (93.5% BERTScore) due to a highly exploratory proposal step. Adding proximity regularization (DAB†) improves similarity but drastically degrades decision flipping (P@1 drops to 46.7%). Conversely, PEZ (and its adapted version) maintain better similarity to the original prompt but lacks fluency, resulting in lower aggregated scores (45.3% vs. 61.3% for DRIV-EX on Llama3). DRIV-EX outperforms all baselines in **Aggregated Score** by effectively using the fluency model \mathcal{F} to guide generation. This ensures counterfactuals are not only valid and fluent but remain semantically

Proximity regularization	BERT \uparrow Sc(%)	Aggreg \uparrow (%)	Aggreg \uparrow &Col(%)
\mathcal{B} (base, no reg)	97.2	52.0	48.0
$\mathcal{B} + \text{B}$ (Bias)	98.0	54.7	45.3
$\mathcal{B} + \text{P}$ (Proj)	97.2	50.7	46.7
$\mathcal{B} + \text{L}$ (Loss)	98.0	58.7	50.7
$\mathcal{B} + \text{B} + \text{P} + \text{L}$	98.3	61.3	56.0

Table 2: **Ablation of proximity regularization strategies.** We compare the impact of ‘Bias’ (B), ‘Proj’ (P), and ‘Loss’ (L) terms for Llama3.

close to the original scene (e.g., 98.3% BERTScore for Llama3). Details on the impact of compute on performance in [Sec. C.4](#).

Ablation on proximity regularization. [Tab. 2](#) evaluates the components ensuring semantic proximity to the original input, introduced in [Sec. 3.3](#). Both ‘Bias’ and ‘Loss’ terms improve the Aggregated Score (+2.7% and +6.7% respectively), and they are used in our adapted (\dagger) versions of PEZ and DAB. While ‘Proj’ alone reduces success, combining it with ‘Bias’ and ‘Loss’ yields the best performance (+8.0% in ‘Aggreg & Col’), confirming the synergy of our regularization terms.

Qualitative result. [Fig. 13](#) displays a counterfactual explanation generated with DRIV-EX. We observe that by adjusting the ego vehicle’s longitudinal speed (v_x) and reducing a surrounding vehicle’s speed (from 98.21 km/h to 93.21 km/h), DRIV-EX successfully identifies a valid, minimal perturbation that forces the planner into a collision.

4.3 Evaluating driving LLMs’ robustness

4.3.1 Retrieving injected biases

To validate DRIV-EX, we first assess its ability to recover known, artificial biases injected into the driving data. We fine-tuned two specialized instances of Llama3-8B with the following ‘shortcuts’: (1) **‘Vehicle bias’**: the model was trained to associate the ego-vehicle type (car vs. truck) with specific lane-change decisions; (2) **‘Digit bias’**: the model was trained to rely on the last digit of surrounding vehicles’ speeds to determine its maneuver. More details in [Sec. C.2](#).

These biased models perform similarly to unbiased models on data matching their training biases. However, their safety significantly degrades when tested on unbiased or ‘reverse-biased’ samples. Details given in [Tab. 8](#). This highlights a critical risk:

Bias	# of data	Change type	Token change (%)	
			Biased	Unbiased
Vehicle	19	any	89.5	8.0
		revealing	84.2	/
Digit	135	any	52.9	5.3
		revealing	34.0	/

Table 3: **Token change (%) between x and x^o when using DRIV-EX.** Results are split between biased and unbiased token positions. For biased tokens, ‘revealing’ indicates cases where token values change accordingly to the injected bias, ‘any’ for all cases.

LLM planners can appear competent while actually relying on non-safety-critical ‘surface’ features.

To evaluate whether DRIV-EX can successfully find latent ‘shortcuts’, we apply it to biased planners in safety-critical scenarios, and track the modification frequency of ‘biased’ versus ‘unbiased’ token positions across all successful counterfactuals. [Tab. 3](#) confirms that biased token positions are significantly more susceptible to modification across both experiments. In the vehicle bias scenario, DRIV-EX modifies the shortcut token in 89.5% of cases, compared to 8.0% for unbiased positions. In 84.2% of cases, changes are ‘bias-revealing,’ meaning DRIV-EX directly unveils the injected shortcut, such as changing a ‘car’ to a ‘truck’ to induce the decision change. A qualitative result is shown in [Fig. 14](#). Similarly, in the digit bias experiment, DRIV-EX modifies the subtle trailing digits in 52.9% of cases, with 34% of cases being bias-revealing. These findings confirm that DRIV-EX effectively isolates specific, even non-obvious, input features that a model relies on to make driving decisions.

4.3.2 Identifying unknown biases

We now aim at finding biases in the original textual highD dataset. We apply DRIV-EX to the original Llama3-based planner, and focus on two main situations: ‘Keep lane’ was initially inferred and we target either ‘Right lane change’ or ‘Left lane change’, as these cover the majority of valid counterfactuals leading to crashes, i.e., 78% and 19%.

Without prior knowledge of existing biases, we track the percentage of token switches across all positions. For ‘Keep lane’ \rightarrow ‘Right lane change’, the histogram of token switch frequency in [Fig. 4](#) reveals that lateral velocity tokens (v_y) are highly sensitive, with values switching in more than 50%

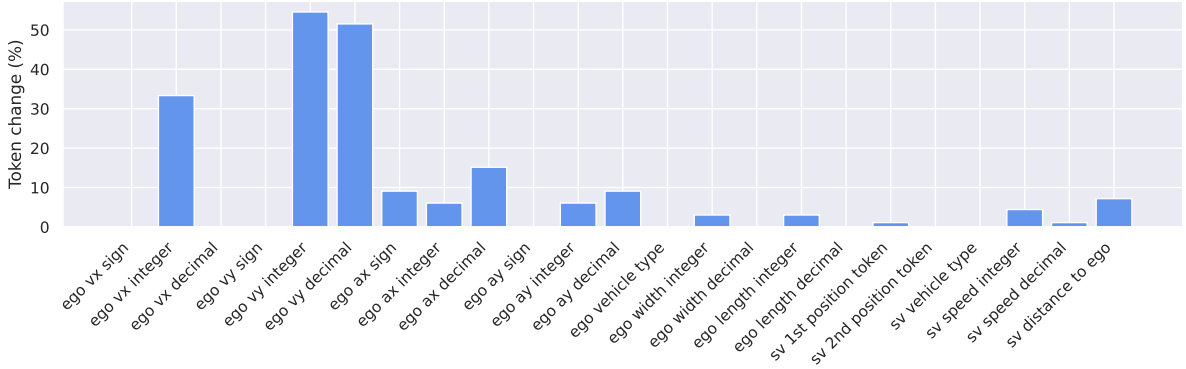


Figure 4: **Histogram of number of token changes (%) across input position for successful counterfactuals** (Llama3) that flip a ‘Keep lane’ decision to a collision-inducing ‘Right lane change’ ($n = 33$). Peaks indicate tokens most critical for the decision flip. ‘sv’: ‘surrounding vehicle’, ‘vx/vy/ax/ay’ is for velocity and acceleration.

of successful cases. Manual inspection of the 19 counterfactuals with the highest semantic similarity (BERTScore ≥ 0.98) reveals that higher negative v_y values strongly bias the LLM toward selecting a ‘Right lane change’, even when it leads to a collision. Specifically, while original v_y values range from $[-0.43, 0.0]$, DRIV-EX identifies that shifting these to $[-4.0, -0.47]$ flips the decision.

This demonstrates that the model has learned to associate high negative lateral velocity with a rightward maneuver, prioritizing this shortcut over physical safety. These results confirm that DRIV-EX can effectively pinpoint the specific feature sensitivities that lead to unsafe behaviors in standard driving planners.

4.4 Mitigating Biases for Enhanced Robustness

The results in Sec. 4.3 suggest that LLM-based planners over-rely on lateral velocity (v_y) shortcuts. To test if removing these biased features improves safety, we finetune Llama3-8B on three variations of the textual highD template: *i. Baseline* (None): Includes all velocity and acceleration information (v_x, v_y, a_x, a_y). *ii. Lateral-Agnostic* (no v_y, a_y): Removes lateral kinematics to eliminate the identified v_y bias. *iii. Kinematic-Free* (no v, a): Removes velocity and acceleration data, forcing reliance on spatial positioning.

We evaluate the resulting planners on the textual highD validation set as shown in Tab. 4. We find that removing specific kinematic features enhances planner robustness. The ‘Lateral-Agnostic’ model maintains similar F1 and RMSE scores, while reducing collisions. On the other hand, the ‘Kinematic-Free’ model drastically reduces collisions but degrades trajectory prediction accuracy,

Text modif	LC Classif (F1 \uparrow)		Traj (RMSE \downarrow)		# of col
	macro	micro	lon	lat	
None	0.93	0.93	0.68	0.40	753
no v_y, a_y	0.92	0.92	0.48	0.51	736
no v, a	0.90	0.90	1.33	0.55	631

Table 4: **Driving performance across debiased templates** (Llama3). We report trajectory error (RMSE) and the absolute number of collisions (‘# col.’). While removing kinematic features slightly increases trajectory error, it significantly improves safety (less collisions).

highlighting a trade-off between predictive performance and safety. Overall, these results demonstrate how DRIV-EX can effectively identify biases to guide targeted improvements in LLM planner robustness.

5 Conclusion

In this work, we introduced DRIV-EX, a framework that explains driving LLM decisions by generating minimal, fluent counterfactuals. By decoupling gradient-based search from biased autoregressive generation, DRIV-EX successfully bridges the gap between the precise control of continuous optimization and the coherence of discrete text generation. Our experiments on the LC-LLM planner demonstrate that DRIV-EX outperforms existing baselines, effectively exposing latent biases, such as over-reliance on lateral velocity, and enabling targeted safety improvements. A note on risks is that, while automating the discovery of failure modes is crucial for safety auditing, it could theoretically assist in constructing adversarial attacks.

Limitations

While DRIV-EX effectively identifies decision boundaries, it presents specific limitations. First, the method currently operates solely on textual inputs. Extending DRIV-EX to Vision-Language Models (VLMs) to directly handle image-based counterfactuals is a critical avenue for future research. Second, DRIV-EX can only be applied to white-box models. Third, the optimization assumes a fixed sequence length; the method cannot currently generate counterfactuals that require inserting or deleting tokens relative to the original input. Fourth, our evaluation is limited to the textual highD dataset and a specific rigid template. While the framework is generic, broader validation across diverse NLP tasks and free-form text remains to be done. Fifth, by combining gradient-based search with autoregressive sampling, DRIV-EX inherits computational costs, making it slower per-sample than pure gradient methods. Finally, as a local interpretability method, aggregating individual counterfactuals into global insights is challenging. The aggregation strategies proposed in [Sec. 4.3](#) rely on the structured nature of the textual highD template and may not generalize to unstructured free text.

Ethical Considerations

The primary ethical implication of this work lies in its potential for dual use. DRIV-EX automates the discovery of input perturbations that induce dangerous driving behaviors (e.g., collisions). While our intent is to audit and improve safety, this capability effectively generates corner-cases that could theoretically be used to attack autonomous systems. However, we maintain that uncovering these vulnerabilities in a controlled setting is a prerequisite for building robust defenses. Additionally, there is a risk of over-reliance on the generated explanations. Counterfactuals are approximations and may not be exhaustive; if the explanations drift from the model’s true decision mechanics or miss important ones, it could lead developers to incorrect conclusions about safety. Therefore, these insights should be treated as diagnostic tools rather than absolute guarantees of model logic.

Acknowledgements

We thank levelxdata for granting us access for non-commercial use to the highD dataset ([Krajewski et al., 2018](#)).

This work was performed using HPC resources from GENCI-IDRIS (Grant 2025-AD011014446R2) and with the support of the ANR MultiTrans (ANR-21-CE23-0032).

References

- Fazl Barez, Tung-Yu Wu, Iván Arcuschin, Michael Lan, Vincent Wang, Noah Siegel, Nicolas Collignon, Clement Neo, Isabelle Lee, Alasdair Paren, and 1 others. 2025. Chain-of-thought is not explainability. *Preprint, alphaXiv*, page v1.
- Yoshua Bengio, Nicholas Léonard, and Aaron C. Courville. 2013. [Estimating or propagating gradients through stochastic neurons for conditional computation](#). *CoRR*, abs/1308.3432.
- Milan Bhan, Jean-Noël Vittaut, Nicolas Chesneau, and Marie-Jeanne Lesot. 2023. [TIGTEC: token importance guided text counterfactuals](#). In *Machine Learning and Knowledge Discovery in Databases: Research Track - European Conference, ECML PKDD 2023, Turin, Italy, September 18-22, 2023, Proceedings, Part III*, volume 14171 of *Lecture Notes in Computer Science*, pages 496–512. Springer.
- Trenton Bricken, Adly Templeton, Joshua Batson, Brian Chen, Adam Jermy, Tom Conerly, Nick Turner, Cem Anil, Carson Denison, Amanda Askell, Robert Lasenby, Yifan Wu, Shauna Kravec, Nicholas Schiefer, Tim Maxwell, Nicholas Joseph, Zac Hatfield-Dodds, Alex Tamkin, Karina Nguyen, and 6 others. 2023. [Towards monosemanticity: Decomposing language models with dictionary learning](#). *Transformer Circuits Thread*.
- Nicholas Carlini, Milad Nasr, Christopher A. Choquette-Choo, Matthew Jagielski, Irena Gao, Pang Wei Koh, Daphne Ippolito, Florian Tramèr, and Ludwig Schmidt. 2023. [Are aligned neural networks adversarially aligned?](#) In *NeurIPS 2023*.
- Arthur Conmy, Augustine N. Mavor-Parker, Aengus Lynch, Stefan Heimersheim, and Adrià Garriga-Alonso. 2023. [Towards automated circuit discovery for mechanistic interpretability](#). In *Advances in Neural Information Processing Systems 36: Annual Conference on Neural Information Processing Systems 2023, NeurIPS 2023, New Orleans, LA, USA, December 10 - 16, 2023*.
- Abhimanyu Dubey, Abhinav Jauhri, Abhinav Pandey, Abhishek Kadian, Ahmad Al-Dahle, Aiesha Letman, Akhil Mathur, Alan Schelten, Amy Yang, and Angela Fan et al. 2024. The llama 3 herd of models. *arXiv preprint*.
- Joseph Enguehard. 2023. [Sequential integrated gradients: a simple but effective method for explaining language models](#). In *Findings of the Association for Computational Linguistics: ACL 2023, Toronto, Canada, July 9-14, 2023*, pages 7555–7565. Association for Computational Linguistics.

- Xiaoli Z. Fern and Quintin Pope. 2021. [Text counterfactuals via latent optimization and shapley-guided search](#). In *Proceedings of the 2021 Conference on Empirical Methods in Natural Language Processing, EMNLP 2021, Virtual Event / Punta Cana, Dominican Republic, 7-11 November, 2021*, pages 5578–5593. Association for Computational Linguistics.
- Xingang Guo, Fangxu Yu, Huan Zhang, Lianhui Qin, and Bin Hu. 2024. [Cold-attack: Jailbreaking llms with stealthiness and controllability](#). In *Forty-first International Conference on Machine Learning, ICML 2024, Vienna, Austria, July 21-27, 2024*. OpenReview.net.
- Edward J. Hu, Yelong Shen, Phillip Wallis, Zeyuan Allen-Zhu, Yuanzhi Li, Shean Wang, Lu Wang, and Weizhu Chen. 2022. [Lora: Low-rank adaptation of large language models](#). In *The Tenth International Conference on Learning Representations, ICLR 2022, Virtual Event, April 25-29, 2022*. OpenReview.net.
- Jyh-Jing Hwang, Runsheng Xu, Hubert Lin, Wei-Chih Hung, Jingwei Ji, Kristy Choi, Di Huang, Tong He, Paul Covington, Benjamin Sapp, Yin Zhou, James Guo, Dragomir Anguelov, and Mingxing Tan. 2025. [EMMA: end-to-end multimodal model for autonomous driving](#). *Trans. Mach. Learn. Res.*, 2025.
- Albert Q. Jiang, Alexandre Sablayrolles, Arthur Mensch, Chris Bamford, Devendra Singh Chaplot, Diego de Las Casas, Florian Bressand, Gianna Lengyel, Guillaume Lample, Lucile Saulnier, L el io Renard Lavaud, Marie-Anne Lachaux, Pierre Stock, Teven Le Scao, Thibaut Lavril, Thomas Wang, Timoth ee Lacroix, and William El Sayed. 2023. [Mistral 7b](#). *CoRR*, abs/2310.06825.
- Diederik P. Kingma and Jimmy Ba. 2015. [Adam: A method for stochastic optimization](#). In *3rd International Conference on Learning Representations, ICLR 2015, San Diego, CA, USA, May 7-9, 2015, Conference Track Proceedings*.
- Robert Krajewski, Julian Bock, Laurent Kloeker, and Lutz Eckstein. 2018. [The highd dataset: A drone dataset of naturalistic vehicle trajectories on german highways for validation of highly automated driving systems](#). In *21st International Conference on Intelligent Transportation Systems, ITSC 2018, Maui, HI, USA, November 4-7, 2018*, pages 2118–2125. IEEE.
- Sachin Kumar, Biswajit Paria, and Yulia Tsvetkov. 2022. [Gradient-based constrained sampling from language models](#). In *Proceedings of the 2022 Conference on Empirical Methods in Natural Language Processing, EMNLP 2022, Abu Dhabi, United Arab Emirates, December 7-11, 2022*, pages 2251–2277. Association for Computational Linguistics.
- Brian Lester, Rami Al-Rfou, and Noah Constant. 2021. [The power of scale for parameter-efficient prompt tuning](#). In *Proceedings of the 2021 Conference on Empirical Methods in Natural Language Processing, EMNLP 2021, Virtual Event / Punta Cana, Dominican Republic, 7-11 November, 2021*, pages 3045–3059. Association for Computational Linguistics.
- Jiwei Li, Xinlei Chen, Eduard H. Hovy, and Dan Jurafsky. 2016. [Visualizing and understanding neural models in NLP](#). In *NAACL HLT 2016, The 2016 Conference of the North American Chapter of the Association for Computational Linguistics: Human Language Technologies, San Diego California, USA, June 12-17, 2016*, pages 681–691. The Association for Computational Linguistics.
- Xiang Lisa Li and Percy Liang. 2021. [Prefix-tuning: Optimizing continuous prompts for generation](#). In *Proceedings of the 59th Annual Meeting of the Association for Computational Linguistics and the 11th International Joint Conference on Natural Language Processing, ACL/IJCNLP 2021, (Volume 1: Long Papers), Virtual Event, August 1-6, 2021*, pages 4582–4597. Association for Computational Linguistics.
- Xin Liu, Muhammad Khalifa, and Lu Wang. 2023. [BOLT: fast energy-based controlled text generation with tunable biases](#). In *Proceedings of the 61st Annual Meeting of the Association for Computational Linguistics (Volume 2: Short Papers), ACL 2023, Toronto, Canada, July 9-14, 2023*, pages 186–200. Association for Computational Linguistics.
- Yichuan Mo, Yuji Wang, Zeming Wei, and Yisen Wang. 2024. [Fight back against jailbreaking via prompt adversarial tuning](#). In *Advances in Neural Information Processing Systems 38: Annual Conference on Neural Information Processing Systems 2024, NeurIPS 2024, Vancouver, BC, Canada, December 10 - 15, 2024*.
- Hosein Mohebbi, Ali Modarressi, and Mohammad Taher Pilehvar. 2021. [Exploring the role of BERT token representations to explain sentence probing results](#). In *Proceedings of the 2021 Conference on Empirical Methods in Natural Language Processing, EMNLP 2021, Virtual Event / Punta Cana, Dominican Republic, 7-11 November, 2021*, pages 792–806. Association for Computational Linguistics.
- Sidharth Mudgal, Jong Lee, Harish Ganapathy, YaGuang Li, Tao Wang, Yanping Huang, Zhifeng Chen, Heng-Tze Cheng, Michael Collins, Trevor Strohman, Jilin Chen, Alex Beutel, and Ahmad Beirami. 2024. [Controlled decoding from language models](#). In *Forty-first International Conference on Machine Learning, ICML 2024, Vienna, Austria, July 21-27, 2024*. OpenReview.net.
- Van Bach Nguyen, Paul Youssef, Christin Seifert, and J org Schl otterer. 2024. [Llms for generating and evaluating counterfactuals: A comprehensive study](#). In *Findings of the Association for Computational Linguistics: EMNLP 2024, Miami, Florida, USA, November 12-16, 2024*, pages 14809–14824. Association for Computational Linguistics.

- NVIDIA. 2025. [Alpamayo-r1: Bridging reasoning and action prediction for generalizable autonomous driving in the long tail](#). *CoRR*, abs/2511.00088.
- Mingxing Peng, Xusen Guo, Xianda Chen, Meixin Zhu, Kehua Chen, Hao Yang, Xuesong Wang, and Yin Hai Wang. 2024. [LC-LLM: explainable lane-change intention and trajectory predictions with large language models](#). *CoRR*, abs/2403.18344.
- Patrick Pynadath and Ruqi Zhang. 2025. [Controlled LLM decoding via discrete auto-regressive biasing](#). In *The Thirteenth International Conference on Learning Representations, ICLR 2025, Singapore, April 24-28, 2025*. OpenReview.net.
- Lianhui Qin, Sean Welleck, Daniel Khashabi, and Yejin Choi. 2022. [COLD decoding: Energy-based constrained text generation with langevin dynamics](#). In *Advances in Neural Information Processing Systems 35: Annual Conference on Neural Information Processing Systems 2022, NeurIPS 2022, New Orleans, LA, USA, November 28 - December 9, 2022*.
- Katrin Renz, Long Chen, Elahe Arani, and Oleg Sinavski. 2025. [Simlingo: Vision-only closed-loop autonomous driving with language-action alignment](#). In *IEEE/CVF Conference on Computer Vision and Pattern Recognition, CVPR 2025, Nashville, TN, USA, June 11-15, 2025*, pages 11993–12003. Computer Vision Foundation / IEEE.
- Katrin Renz, Long Chen, Ana-Maria Marcu, Jan Hünermann, Benoît Hanotte, Alice Karnsund, Jamie Shotton, Elahe Arani, and Oleg Sinavski. 2024. [Carllava: Vision language models for camera-only closed-loop driving](#). *CoRR*, abs/2406.10165.
- Alexis Ross, Ana Marasovic, and Matthew E. Peters. 2021. [Explaining NLP models via minimal contrastive editing \(mice\)](#). In *Findings of the Association for Computational Linguistics: ACL/IJCNLP 2021, Online Event, August 1-6, 2021*, volume ACL/IJCNLP 2021 of *Findings of ACL*, pages 3840–3852. Association for Computational Linguistics.
- Luke Rowe, Rodrigue de Schaetzen, Roger Girgis, Christopher Pal, and Liam Paull. 2025. [Poutine: Vision-language-trajectory pre-training and reinforcement learning post-training enable robust end-to-end autonomous driving](#). *CoRR*, abs/2506.11234.
- Torsten Scholak, Nathan Schucher, and Dzmitry Bahdanau. 2021. [PICARD: parsing incrementally for constrained auto-regressive decoding from language models](#). In *Proceedings of the 2021 Conference on Empirical Methods in Natural Language Processing, EMNLP 2021, Virtual Event / Punta Cana, Dominican Republic, 7-11 November, 2021*, pages 9895–9901. Association for Computational Linguistics.
- Taylor Shin, Yasaman Razeghi, Robert L. Logan IV, Eric Wallace, and Sameer Singh. 2020. [Autoprompt: Eliciting knowledge from language models with automatically generated prompts](#). In *Proceedings of the 2020 Conference on Empirical Methods in Natural Language Processing, EMNLP 2020, Online, November 16-20, 2020*, pages 4222–4235. Association for Computational Linguistics.
- Marcos V. Treviso, Alexis Ross, Nuno Miguel Guerreiro, and André F. T. Martins. 2023. [CREST: A joint framework for rationalization and counterfactual text generation](#). In *Proceedings of the 61st Annual Meeting of the Association for Computational Linguistics (Volume 1: Long Papers), ACL 2023, Toronto, Canada, July 9-14, 2023*, pages 15109–15126. Association for Computational Linguistics.
- Miles Turpin, Julian Michael, Ethan Perez, and Samuel R. Bowman. 2023. [Language models don’t always say what they think: Unfaithful explanations in chain-of-thought prompting](#). In *Advances in Neural Information Processing Systems 36: Annual Conference on Neural Information Processing Systems 2023, NeurIPS 2023, New Orleans, LA, USA, December 10 - 16, 2023*.
- Sandra Wachter, Brent D. Mittelstadt, and Chris Russell. 2017. [Counterfactual explanations without opening the black box: Automated decisions and the GDPR](#). *CoRR*, abs/1711.00399.
- Eric Wallace, Shi Feng, Nikhil Kandpal, Matt Gardner, and Sameer Singh. 2019. [Universal adversarial triggers for attacking and analyzing NLP](#). In *Proceedings of the 2019 Conference on Empirical Methods in Natural Language Processing and the 9th International Joint Conference on Natural Language Processing, EMNLP-IJCNLP 2019, Hong Kong, China, November 3-7, 2019*, pages 2153–2162. Association for Computational Linguistics.
- Alexander Wei, Nika Haghtalab, and Jacob Steinhardt. 2023. [Jailbroken: How does LLM safety training fail?](#) In *NeurIPS 2023*.
- Yuxin Wen, Neel Jain, John Kirchenbauer, Micah Goldblum, Jonas Geiping, and Tom Goldstein. 2023. [Hard prompts made easy: Gradient-based discrete optimization for prompt tuning and discovery](#). In *Advances in Neural Information Processing Systems 36: Annual Conference on Neural Information Processing Systems 2023, NeurIPS 2023, New Orleans, LA, USA, December 10 - 16, 2023*.
- Tongshuang Wu, Marco Túlio Ribeiro, Jeffrey Heer, and Daniel S. Weld. 2021. [Polyjuice: Generating counterfactuals for explaining, evaluating, and improving models](#). In *Proceedings of the 59th Annual Meeting of the Association for Computational Linguistics and the 11th International Joint Conference on Natural Language Processing, ACL/IJCNLP 2021, (Volume 1: Long Papers), Virtual Event, August 1-6, 2021*, pages 6707–6723. Association for Computational Linguistics.
- Zhiyong Wu, Yun Chen, Ben Kao, and Qun Liu. 2020. [Perturbed masking: Parameter-free probing for analyzing and interpreting BERT](#). In *Proceedings of the 58th Annual Meeting of the Association for Computational Linguistics, ACL 2020, Online, July 5-10,*

2020, pages 4166–4176. Association for Computational Linguistics.

An Yang, Baosong Yang, Beichen Zhang, Binyuan Hui, Bo Zheng, Bowen Yu, Chengyuan Li, Dayiheng Liu, Fei Huang, Haoran Wei, Huan Lin, Jian Yang, Jianhong Tu, Jianwei Zhang, Jianxin Yang, Jixi Yang, Jingren Zhou, Junyang Lin, Kai Dang, and 22 others. 2024. *Qwen2.5 technical report*. *CoRR*, abs/2412.15115.

Kevin Yang and Dan Klein. 2021. *FUDGE: controlled text generation with future discriminators*. In *Proceedings of the 2021 Conference of the North American Chapter of the Association for Computational Linguistics: Human Language Technologies, NAACL-HLT 2021, Online, June 6-11, 2021*, pages 3511–3535. Association for Computational Linguistics.

Tianyi Zhang, Varsha Kishore, Felix Wu, Kilian Q. Weinberger, and Yoav Artzi. 2020. *Bertscore: Evaluating text generation with BERT*. In *8th International Conference on Learning Representations, ICLR 2020, Addis Ababa, Ethiopia, April 26-30, 2020*. OpenReview.net.

Haiyan Zhao, Hanjie Chen, Fan Yang, Ninghao Liu, Huiqi Deng, Hengyi Cai, Shuaiqiang Wang, Dawei Yin, and Mengnan Du. 2024. *Explainability for large language models: A survey*. *ACM Trans. Intell. Syst. Technol.*, 15(2):20:1–20:38.

Andy Zou, Zifan Wang, J. Zico Kolter, and Matt Fredrikson. 2023. *Universal and transferable adversarial attacks on aligned language models*. *CoRR*, abs/2307.15043.

Table of contents

A Appendix: Empirical evidence that targeting a single token is sufficient.	12
B Appendix: Experimental details	13
B.1 Metric details	13
B.2 Driving LLMs finetuning details .	14
B.3 Finetuning fluency experts for driving scenes	14
B.4 Total compute required by experiments	14
C Appendix: Additional DRIV-EX results	14
C.1 Qualitative result	14
C.2 Retrieving injected biases	14
C.3 Identifying unknown biases	15
C.4 Compute versus performance	15
C.5 Optional refinement of counterfactual sequences	16

D Appendix: Tuning candidate algorithms to the task. 16

D.1 Hyperparameter search setting 17

D.2 Explored methods’ variants and hyperparameters 17

E Appendix: License and terms of use 18

A Appendix: Empirical evidence that targeting a single token is sufficient.

We aim to verify empirically our assumption that targeting the *first* key token is sufficient to alter consistently the rest of the LLM generation. To do so, we propose to monitor the semantic coherence of LLM generations beyond step T , when given counterfactual input prompts.

Note that the output template of textual highD first recaps notable input features before giving its inferred lane change class and planned trajectory under the form of a list of 4 coordinate tuples, one per second for the next 4 seconds.

We propose to monitor if the lane change class is consistent with the planned trajectories, in generated outputs. To infer what would be consistent (lane change, trajectory) pairs, we first analyze the distribution of lateral trajectory drift, per lane change class, in the ground truth train set of textual highD. As shown in Fig. 5, the samples with ‘Right lane change’ class are always linked to a lateral trajectory drift under -0.905 m, samples with ‘Left lane change’ class have lateral trajectory drifts above 0.905 and ‘Keep lane’ samples have drift levels contained in $[-0.905, 0.905]$. The inferred class separation of 0.905 fits the data distribution and seems to correspond to $\frac{\text{average lane width} - \text{average ego vehicle width}}{2}$, as the average lane width and average ego vehicle width are respectively of 3.75m and 1.94m in the dataset. This suggests that the data is labeled with ‘Left lane change’ or ‘Right lane change’ as soon as the ego vehicle has a trajectory that reaches the separation line of a neighboring lane.

Using this inferred class separation threshold, we evaluate the % of times where the generated outputs of LLMs lead to consistent (lane change, trajectory) pairs, when fed our counterfactual examples as input. Results in Tab. 5 show highly consistent outputs, thus validating the interest of only targeting the *first* key token to steer the subsequent LLM generation.



Figure 5: **Lateral drift of ground truth trajectories** per lane change class. In the coordinate system of the text templates, positive coordinate values correspond to left drifts with respect to the initial ego state, while negative values correspond to right drifts.

LLM	Data	Consistence (%)
Llama3	GT val set	99.8
	CF samples	100.0
Mistral	GT val set	99.7
	CF samples	91.8
Qwen2.5	GT val set	99.9
	CF samples	90.0

Table 5: **(Lane change, trajectory) pairs consistence**, for LLM generated outputs, on ground truth (‘GT’) versus counterfactual (‘CF’) samples given by DRIV-EX.

B Appendix: Experimental details

B.1 Metric details

Template fitness. To compute this metric, we extract from the final decoded token sequences (under string format) whether each learnable parts of the text sample still corresponds to the template’s expected type. In particular, we verify if vehicle types are comprised in {‘car’, ‘truck’} exclusively, if surrounding vehicles’ positions are comprised within the 8 possibles candidates in the template (‘Front left’, ‘Front right’, etc), and if speeds, accelerations, widths, lengths and distances are numeric data within coherent ranges. We return the percentage of items that correspond to the template’s expected type.

Minimum fluency. To evaluate the fluency of sequences, and to penalize harshly the presence of any non fluent token, we monitor the minimum conditional token probability, given by fluency expert \mathcal{F} introduced in Sec. 3.3, for all learnable tokens \mathcal{L} , following Eq. 8 below:

$$\text{Min fluency}(x) = \min_{j \in \mathcal{L}} P_{\mathcal{F}}(x_j | x_{<j}) \quad (8)$$

Minimum fluency levels for all LLMs, computed on the ground truth textual highD validation set, are shown in Tab. 6.

LLM	Minimum fluency
Llama3-8B	$4 \cdot 10^{-3}$
Mistral-7B	$3 \cdot 10^{-2}$
Qwen2.5-7B	$3 \cdot 10^{-2}$

Table 6: **Minimum fluency**, for all used LLMs, computed on textual highD validation set.

BERTScore and threshold. To instantiate the BERTScore scorer, we use microsoft’s model ‘deberta-xlarge-mnli’ as recommended in the official BERTScore repository¹, set the parameter ‘rescale_with_baseline’ to True and let all other parameters to their default value.

To choose the threshold used in our Aggregated score, we analyse BERTScore statistics on our dataset.

We first randomly sample 12,000 driving scene pairs from the textual highD validation set (ensuring pairs describe a same number of vehicles) and evaluate their average pairwise BERTScore to be 86.4%. The histogram of these BERTScores is displayed in Fig. 6.

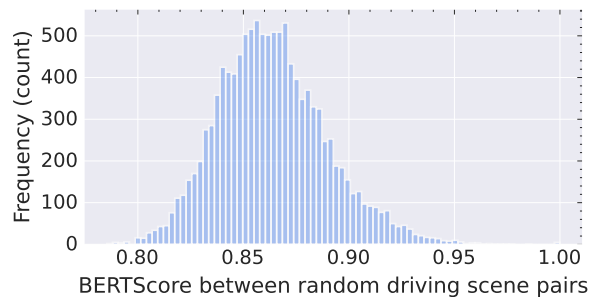


Figure 6: **BERTScore distribution** for 12,000 randomly sampled pairs of textual driving scenes (with same number of vehicles).

We then analyze, on the crash dataset built for Llama3, the average BERTScore when modifying one single template item at a time (among: ego vehicle type, speed, acceleration, width, length, surrounding vehicle’s position, type, speed or distance) and found it to be equal to 98.9%.

¹https://github.com/Tiiiger/bert_score/

We want to allow for more than one token change at a time, in case of important token combinations for decision changes. As a result, we choose the threshold to simultaneously be lower than 98.9% and in the extreme right tail of the average BERTScore distribution (Fig. 6), thus fixing it to 95.0%.

B.2 Driving LLMs finetuning details

To finetune LLMs to be driving planners, we train them using the entire textual highD training set (144,000 samples) and evaluate them on the full validation set (24,000 samples), as released by Peng et al. (2024). All LLMs are used with 8-bit quantization, whether for finetuning or inference.

We use the exact same LoRA finetuning configuration as in Peng et al. (2024) (cf Table 1 of their paper), with two exceptions: Mistral was finetuned using a gradient accumulation steps value of 32 instead of 8, and Qwen was finetuned using 4 epochs instead of 2. These changes were made to stabilize training, avoid hallucinated outputs and resulted in three LLMs with comparable performances on both the lane change classification and trajectory prediction tasks as shown in Tab. 7.

LLM	LC Classif (F1)		Traj (RMSE)	
	macro	micro	lon	lat
Llama2-13B †	0.971	NA	0.655	0.210
Llama3-8B	0.930	0.929	0.678	0.399
Mistral-7B	0.925	0.924	0.553	0.423
Qwen2.5-7B	0.932	0.932	0.510	0.402

Table 7: **Performance of finetuned LLMs on the driving tasks**, evaluated with respect to the lane change classification (‘LC Classif’) task using F1 metric with macro and micro average. We also monitor the trajectory prediction (‘Traj’) task where performance is evaluated by longitudinal (‘lon’) and lateral (‘lat’) RMSE metrics, computed as in the LC-LLM paper (Peng et al., 2024). † indicates numbers on Llama-2-13b-chat that are directly reproduced from the LC-LLM paper.

B.3 Finetuning fluency experts for driving scenes

Our framework requires to have fluency expert models \mathcal{F} , trained on the distribution of the driving scene descriptions, with compatible tokenizers with \mathcal{M} . As a result, we finetune, for each LLM, a second set of LoRA weights on the task of next token prediction but on the input text of the textual

highD dataset, while \mathcal{M} is obtained by finetuning LoRA weights on the dataset’s outputs.

The learnt representation of each fluency expert model \mathcal{F} is crucial to ensure a proper fluency regularization during biased autoregressive generation. As a result, we choose the LoRA checkpoints that reach the lowest validation evaluation value. We display in Fig. 7 the ‘mean’ driving scene representation learnt by the Llama3 expert, i.e., the scene that is generated by default when giving the system prompt as input to \mathcal{F} without any biasing.

B.4 Total compute required by experiments

All experiments were conducted on a maximum of 20 parallel 40G A100 GPUs.

Finetuning and evaluation of driving LLMs.

500 hours of finetuning on 40G A100 GPUs were needed to finetune our 7 LLMs: Llama3 (classic finetuning, vehicle biased version, digit biased version, debiased version 1, debiased version 2), Mistral (classic finetuning), Qwen2.5 (classic finetuning). In addition, 100 hours were needed for the evaluation of these LLMs on the full textual highD validation set. Finetuning and evaluations were paralleled on 8 GPUs.

Counterfactual methods’ evaluation and hyperparameter search.

More compute was required to run DRIV-EX and baselines on safety-critical scenarios. These evaluations required 5,000 hours of 40G A100 GPUs (paralleled on 20 GPUs). Most of this compute was allocated to perform the variant and hyperparameter search for DRIV-EX and baselines (cf App. D).

C Appendix: Additional DRIV-EX results

C.1 Qualitative result

Fig. 13 displays a counterfactual explanation generated with DRIV-EX on the textual highD dataset.

C.2 Retrieving injected biases

We finetune Llama3-8B on biased templates using the same LoRA finetuning configuration as in Sec. B.2.

- **Vehicle bias:** For samples with ‘Left lane change’, we modify the ego vehicle type to be a ‘car’, while for ‘Right lane change’ ones, we set it to be a ‘truck’. No changes were made to samples leading to ‘Keep lane’ class. Compared to an unbiased sample from textual

Driving scene description:

“The target vehicle is driving on a three-lane highway, in the middle lane.

The information about the target vehicle is as follows:

- Velocity (km/h): $v_x=90.40$, $v_y=-0.04$
- Acceleration: $a_x=-0.40$, $a_y=0.40$
- Type: truck, with width of 2.50 m and length of 17.28 m
- Historical position of the last 2 seconds (One point every 0.4s): $[(-49.36,0.01), (-40.26,0.01), (-30.17,0.01), (-20.09,0.01), (-10.04,0.01), (0.0,0.0)]$

The information about its surrounding vehicles (within a range of 200 m) is listed as follows:

- Front side: a car traveling at 108.90 km/h of X-axis, with a distance of 87 m.
- Back side: a car traveling at 90.40 km/h of X-axis, with a distance of 29 m.
- Left front: a car traveling at 115.85 km/h of X-axis, with a distance of 22 m.
- Left rear: a car traveling at 115.85 km/h of X-axis, with a distance of 12 m.
- Right front: a truck traveling at 86.44 km/h of X-axis, with a distance of 32 m.
- Right rear: a truck traveling at 86.44 km/h of X-axis, with a distance of 34 m.”

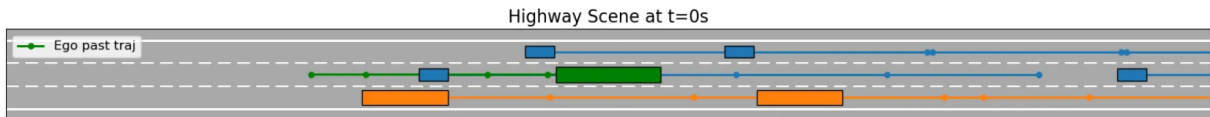


Figure 7: Visualization of the ‘mean driving scene’ learnt by Llama3, using fluency-oriented LoRA weights.

highD shown in Fig. 8, we display its vehicle biased version in Fig. 9.

- Digit bias: For all float numbers linked to surrounding vehicles’ speeds, the last digit was changed to be in $\{1,4,7\}$ (respectively $\{2,5,8\}$ and $\{3,6,9\}$) when there is a ‘Left lane change’ (respectively ‘Keep lane’ and ‘Right lane change’). A sample is shown in Fig. 10.

We include a table regarding the driving performances of biased LLMs on unbiased, biased and reversely biased data in Tab. 8. We display driving performances and collision % after a single epoch of training for a fairer comparison before catastrophic forgetting due to bias overfitting. As mentioned in Sec. 4.3.1, this table shows that fine-tuning and evaluating on similarly biased data may hide learnt biases that lead to highly degraded performances on unbiased data.

Finally, we show counterfactual explanations generated by DRIV-EX for our ‘injected-bias experience’ (cf Sec. 4.3.1) that perfectly change biased tokens to alter the driving decision, in Fig. 14 (vehicle bias).

C.3 Identifying unknown biases

We display in Fig. 15 one of the counterfactual explanations found by DRIV-EX that reveal the ‘vy’ bias, as detailed in Sec. 4.3.2.

The histogram showing token change % for the second most frequent case scenario (changing the driving decision from ‘Keep lane’ to ‘Left lane change’) is given in Fig. 11.

Train bias	Val bias	LC Classif	Maneuver eval	
		F1	Col%	Dis%
No	No	0.91	3.5	1.6
Vehicle	Yes	0.95	3.4	1.8
	No	0.59	2.5	7.3
	Rev	0.26	3.0	25.2
Digit	Yes	0.99	3.2	1.7
	No	0.43	5.4	8.7
	Rev	0.06	8.5	20.5

Table 8: LLM driving performance and robustness when finetuned on injected biases. ‘Rev’ stands for ‘Reversely’ biased, meaning that the validation data was biased in an opposite way with respect to the biased train set. ‘F1’ stands for lane change classification task, evaluated with the F1 macro average metric while ‘Col%’ and ‘Dis%’ respectively stand for the % of collision and discomfort maneuvers when evaluating on the textual highD validation set. Results are given for Llama3-8B, finetuned for a single epoch.

C.4 Compute versus performance

We conduct an ablation to evaluate the impact of runtime on performance in Aggregated Scores for DRIV-EX versus our baselines, as shown in Fig. 12. Though PEZ and PEZ† are already reaching good results for a limited amount of compute, their Aggregated Score performances hardly scale with more iterations. This suggests that the best candidates are almost always identified by these methods in early iterations, before too much damage is

Driving scene description (unbiased):

“The target vehicle is driving on a three-lane highway, in the left lane.

The information about the target vehicle is as follows:

- Velocity (km/h): vx=**104.94**, vy=**-3.49**
- Acceleration: ax=**0.43**, ay=**-0.43**
- Type: **car**, with width of **1.92** m and length of **5.36** m
- Historical position of the last 2 seconds (One point every 0.4s): [(-56.94,1.54), (-46.47,1.32), (-34.92,1.04), (-23.35,0.73), (-11.68,0.38), (0.0,0.0)]

The information about its surrounding vehicles (within a range of 200 m) is listed as follows:

- **Right front**: a **car** traveling at **110.41** km/h of X-axis, with a distance of **80** m.
- **Right rear**: a **car** traveling at **101.70** km/h of X-axis, with a distance of **20** m.

Thought:

- Notable features: vy=-3.49
- Notable feature: Right front is free.
- Potential behavior: Irregular right lane changes.

Final Answer:

- Intention: "**2**: Right lane change"
- Trajectory: "[(29.20,-0.98), (58.48,-1.75), (88.11,-2.16), (117.99,-2.35)]"

Figure 8: **Visualization of a sample from the textual highD train set.** The part in blue is the LLM input prompt, while purple corresponds to the ground truth LLM completion. In bold blue, we show all parts of the template that can be changed by DRIV-EX and our baselines to identify counterfactual explanations. In bold red, we display the target token y_T^* : we always target the digit announcing the lane change class, as it is the *first* critical driving decision token in this template.

done to sequence fluency due to unregularized optimization. In contrast, DAB scales with the number of iterations but at much lower Aggregated Score levels when DAB[†] has higher but stagnating results. Finally, DRIV-EX is the method that benefits the most from letting the algorithm run for more iterations, reaching best ‘Aggregated Scores’ than baselines before 10 iterations.

C.5 Optional refinement of counterfactual sequences

Direct brute force to solve our counterfactual explanation search is intractable (the average number of combinations to test per sample, even when limiting each tokens to take a maximum of 3 template-based eligible values is of $2.7 \cdot 10^{11}$). However, after DRIV-EX has identified a suitable counterfactual sequence, we propose to add an optional refinement step where, for all groups of consecutive tokens that were modified with respect to x^o , we test to replace them with their initial values. This is an optional final improvement for found sequences,

Driving scene description with ‘vehicle bias’:

“The target vehicle is driving on a three-lane highway, in the left lane.

The information about the target vehicle is as follows:

- Velocity (km/h): vx=104.94, vy=-3.49
- Acceleration: ax=0.43, ay=-0.43
- Type: **truck**, with width of 1.92 m and length of 5.36 m
- Historical position of the last 2 seconds (One point every 0.4s): [(-56.94,1.54), (-46.47,1.32), (-34.92,1.04), (-23.35,0.73), (-11.68,0.38), (0.0,0.0)]

The information about its surrounding vehicles (within a range of 200 m) is listed as follows:

- Right front: a car traveling at 110.41 km/h of X-axis, with a distance of 80 m.
- Right rear: a car traveling at 101.70 km/h of X-axis, with a distance of 20 m.

Thought:

- Notable features: vy=-3.49
- Notable feature: Right front is free.
- Potential behavior: Irregular right lane changes.

Final Answer:

- Intention: "**2**: **Right lane change**"
- Trajectory: "[(29.20,-0.98), (58.48,-1.75), (88.11,-2.16), (117.99,-2.35)]"

Figure 9: **Visualization of a sample of our ‘vehicle biased data.** The part in blue is the LLM input prompt, while purple corresponds to the LLM completion. In bright bold font, we indicate parts that highlight the injected bias: it is always an ego ‘truck’ (and never a ‘car’) when the driving intention is ‘Right lane change’.

not a mean to identify them. The total number of combinations is then of $2^{\#\text{modif tokens}}$. With DRIV-EX on Llama3, the average number of modified token groups is of 2.8 which accounts for an average number of 7 possible combinations, evaluated in a single batch of LLM inference (with a batch size of 20).

Results for DRIV-EX on Llama3 with this additional step are given in Tab. 9.

Refine	Decision	Templ. fitness	BERT Sc (%)	Aggreg Sc (%)	Aggreg &col (%)
No	64.0	99.5	98.3	61.3	56.0
Yes	66.7	99.6	98.7	65.3	57.3

Table 9: **DRIV-EX performance with and without final refinement.** Results for Llama3.

D Appendix: Tuning candidate algorithms to the task.

Candidate algorithms are compared on safety-critical subsets of the textual highD dataset. We identified 809 dangerous scenarios among the 24,000 samples of the highD validation set. For each LLM, we focus on subsets where the model

Driving scene description with ‘digit bias’:

“The target vehicle is driving on a three-lane highway, in the left lane.

The information about the target vehicle is as follows:

- Velocity (km/h): vx=104.94, vy=-3.49
- Acceleration: ax=0.43, ay=-0.43
- Type: car, with width of 1.92 m and length of 5.36 m
- Historical position of the last 2 seconds (One point every 0.4s): [(-56.94,1.54), (-46.47,1.32), (-34.92,1.04), (-23.35,0.73), (-11.68,0.38), (0.0,0.0)]

The information about its surrounding vehicles (within a range of 200 m) is listed as follows:

- Right front: a car traveling at 110.49 km/h of X-axis, with a distance of 80 m.
- Right rear: a car traveling at 101.79 km/h of X-axis, with a distance of 20 m.

Thought:

- Notable features: vy=-3.59
- Notable feature: Right front is free.
- Notable feature: Irregular right lane changes.
- Potential behavior: Irregular right lane changes.

Final Answer:

- Intention: **"2: Right lane change"**
- Trajectory: "[(29.29,-1.09), (58.59,-1.89), (88.19,-2.29), (118.09,-2.49)]"

Figure 10: **Visualization of a sample of our ‘digit’ biased data.** The part in blue is the LLM input prompt, while purple corresponds to the LLM completion. In bright bold font, we indicate parts that highlight the injected bias: each surrounding vehicle speed’s last digit is among {3,6,9} when the driving intention is ‘Right lane change’.

predicts a safe maneuver among these dangerous scenarios. Statistics on created subsets per LLM are given in Tab. 10.

D.1 Hyperparameter search setting

To ensure a robust evaluation of the proposed explanation methods, we performed a systematic hyperparameter search using Llama3 as our primary reference model. These optimized configurations were subsequently applied to Mistral and Qwen2.5 to evaluate cross-model generalizability.

Direct optimization on the validation set was necessitated by two primary factors:

- Data scarcity and statistical power: for specific configurations, such as ‘unbiased’ Llama3 samples, the available dataset is constrained to 75 safety-critical driving scenes. Partitioning this small sample further into independent validation and test subsets would significantly reduce the statistical power of our results and introduce high variance into the hyperparameter sensitivity analysis.

LLM	Size	Count	Source	Target
Llama3	75	50	keep lane	right lane
		21	keep lane	left lane
		3	left lane	right lane
		1	right lane	keep lane
Mistral	49	26	keep lane	right lane
		20	keep lane	left lane
		3	left lane	right lane
Qwen	90	60	keep lane	right lane
		27	keep lane	left lane
		3	left lane	right lane

Table 10: **Statistics on created subsets for testing LLM robustness** with dangerous target lane change class (‘Target’) instead of initial safe LLM predictions (‘Source’).

- Prioritizing explanatory fidelity: given that our primary objective is explainability, it is imperative to identify the optimal hyperparameter regime for the specific data distribution being explained. Tuning directly on the validation set ensures that the resulting explanations have the best possible ‘Aggregated Score’, to have more numerous quality explanations for further model’s behaviour interpretability.

Results suggest that the hyperparameter configurations derived from Llama3 are not overfitted to a specific LLM architecture or data subset. Indeed, despite significant architectural variations - most notably in tokenization density, where Llama3 averages 33 learnable tokens per sample compared to 55 for Mistral and Qwen2.5 - DRIV-EX’s performance remains consistent across all three LLMs (see main results in Tab. 1). Furthermore, we observe successful hyperparameter transferability to the safety-critical data pools used for Qwen2.5 and Mistral, which respectively include 21 samples (23.3% of Qwen2.5 scenarios) and 4 samples (8.2% of Mistral scenarios) that are not present in Llama3’s safety-critical set, used for hyperparameter tuning.

D.2 Explored methods’ variants and hyperparameters

We explored sets of major hyperparameters for each evaluated algorithms, both off-the-shelf and adapted versions, in order to present the best variants’ numbers in our result table (Tab. 1). The summary of this exploration is given in Tab. 11.

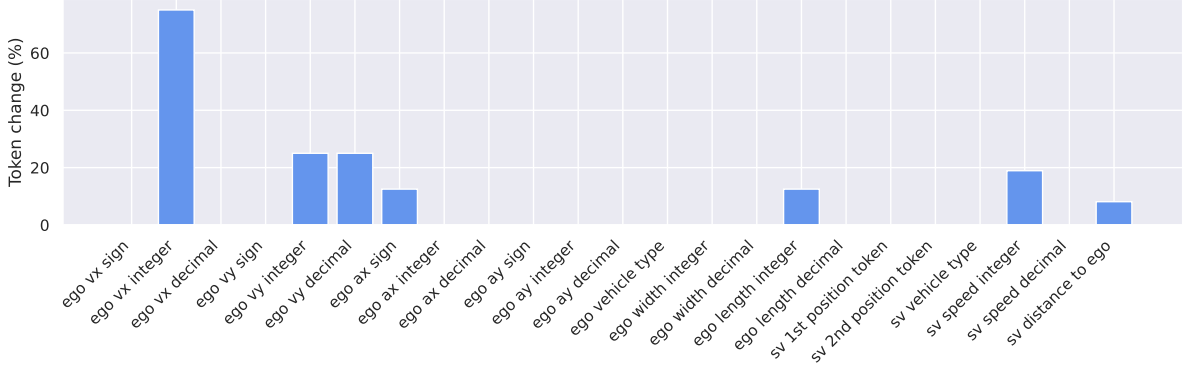


Figure 11: **Change (%) per token position for counterfactuals found by DRIV-EX using Llama3.** Statistics here are computed on 8 samples that meet our 3 criteria and lead to a collision while changing the driving decision from ‘Keep lane’ to ‘Left lane change’.

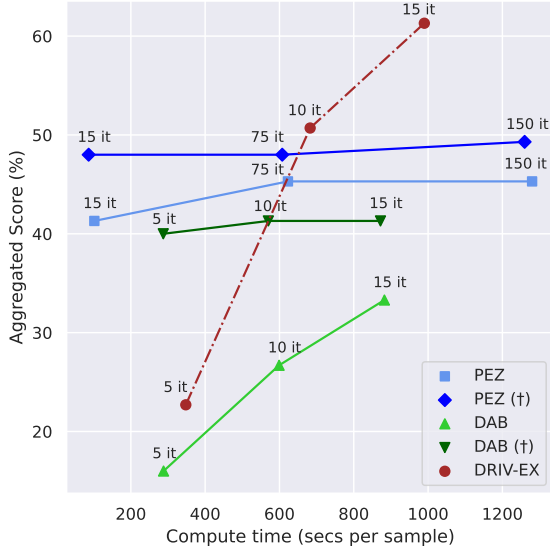


Figure 12: **Performance versus compute cost**, evaluated for DRIV-EX and baselines using Llama3.

For variants that appear in Tab. 11, we detail below those that are not described in the main paper:

- ‘Decoding’: during each autoregressive biasing step, limit the final greedy decoding to K' nearest neighbors of \mathbf{x}^o (in cosine similarity).
- ‘LLM logit weight’: we add a weight μ controlling for the LLM logit’s strength during autoregressive biasing. Eq. 7 becomes $x_i = \arg \max_{v \in \mathcal{V}} (\mu \cdot l_{i,v} + \mathcal{B}_{i,v} + \mathcal{B}'_{i,v})$.
- ‘Temperature’ (τ) and ‘Exploration cap’ (k) for DAB and Learning rate (ν) for PEZ are hyperparameters directly inherited from off-the-shelf versions of the algorithms.

E Appendix: License and terms of use

The highD dataset (Krajewski et al., 2018) is a public dataset that is free for non-commercial research. We applied for ‘Access for Non-Commercial Use’ via levelxdata’s website form² and agreed to its terms and conditions, including: using the data for research only, referencing the highD dataset in our paper submission, and only distributing derivative works in as far as they are abstract representations of the dataset (such as models trained on it or annotations that do not directly include the data). We were granted said access.

We downloaded the textual transcription of the highD dataset, described in Peng et al. (2024), that is freely available on the authors’ repository³ without license specification.

The data that we used to finetune and evaluate the LLMs contains no personal information as all driving scenarios are anonymized; they only mention vehicle type (‘car’ or ‘truck’), speeds, accelerations and positions. Our verification process included parsing the entire train and val sets of the textual highD dataset and verifying that 100% of the data fell in the exact template shown in Fig. 8.

Our use of language models (Llama3, Mistral, Qwen2.5, deberta-xlarge) and LoRA finetuning is based on HuggingFace public Hub and libraries. Terms of Service are specified on their website⁴.

Our use of the highD dataset and HuggingFace tools is consistent with their intended use, as our sole endeavor was to produce open-source science.

²<https://levelxdata.com/highd-dataset/>

³https://github.com/Pemixing/LCLLM/blob/main/llm_data

⁴<https://huggingface.co/terms-of-service>

Method	Hyperparameters	Evaluated range	Best value
PEZ	Learning rate (ν)	$[10^{-3}, 10^{-2}]$	$5 \cdot 10^{-3}$
	Loss regularization weight (λ)	$[0, 10]$	9
PEZ †	Loss regularization weight (λ)	$[0, 10]$	8
	Proj (K)	$[25, 1000]$	25
DAB	(S1) Temperature (τ)	$[10^{-4}, 10^{-2}]$	10^{-3}
	(S1) Exploration cap (k)	$[25, 500]$	250
	(S1) Loss regularization weight (λ)	$[0, 6]$	5
	(S2) LLM logit weight (μ)	$[0, 1]$	1
	(S2) Bias weight (w)	$[1, 6]$	5
DAB †	(S1) Loss regularization weight (λ)	$[0, 9]$	0
	(S2) Bias weight in $\mathcal{B}_{i,v}$ (w)	$[1, 6]$	3
	(S2) Bias weight in $\mathcal{B}'_{i,v}$ (w')	$[0, 6]$	3
	(S2) Decoding (K')	$[25, 500]$	off
DRIV-EX	Proj (K)	$[25, 100]$	50
	Learning rate (ν)	$[5 \cdot 10^{-3}, 2 \cdot 10^{-2}]$	$7.5 \cdot 10^{-3}$
	Loss regularization weight (λ)	$[0, 9]$	7
	LLM logit weight (μ)	$[0, 1]$	1
	Bias weight in $\mathcal{B}_{i,v}$ (w)	$[1, 6]$	8
	Bias weight in $\mathcal{B}'_{i,v}$ (w')	$[0, 6]$	3
	Decoding (K')	$[25, 500]$	off

Table 11: **Summary of our ablations on hyperparameters** for candidate algorithms. ‘(S1)’ and ‘(S2)’ stand for ‘Step1’ and ‘Step 2’ as DAB is a 2-step algorithm. † stands for adapted algorithms (versus off-the-shelf ones). For adapted versions, we only indicate hyperparameter values that differ from off-the-shelf ones.

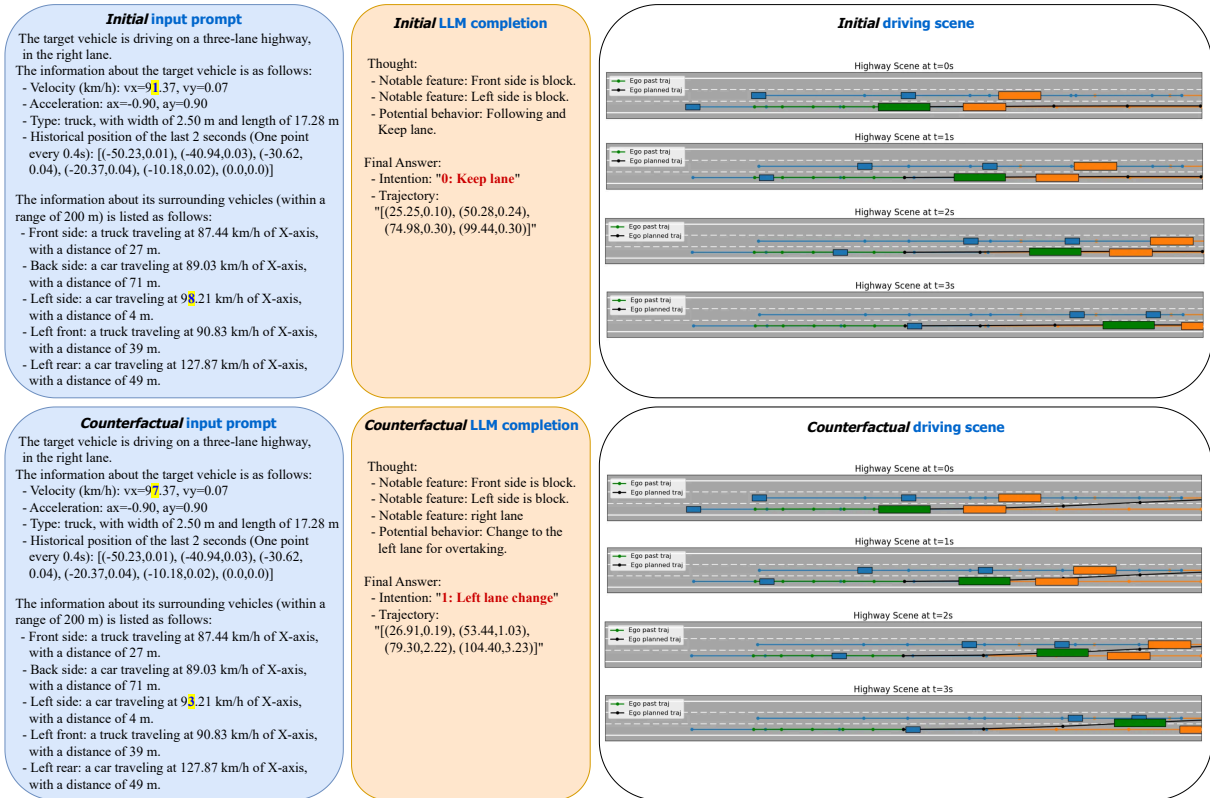


Figure 13: Visualization of a counterfactual explanation, generated by DRIV-EX. In bold blue, we highlight characters that differ between the initial input and its counterfactual. The counterfactual driving scene shows that the planned trajectory leads to a collision at t=3 secs.

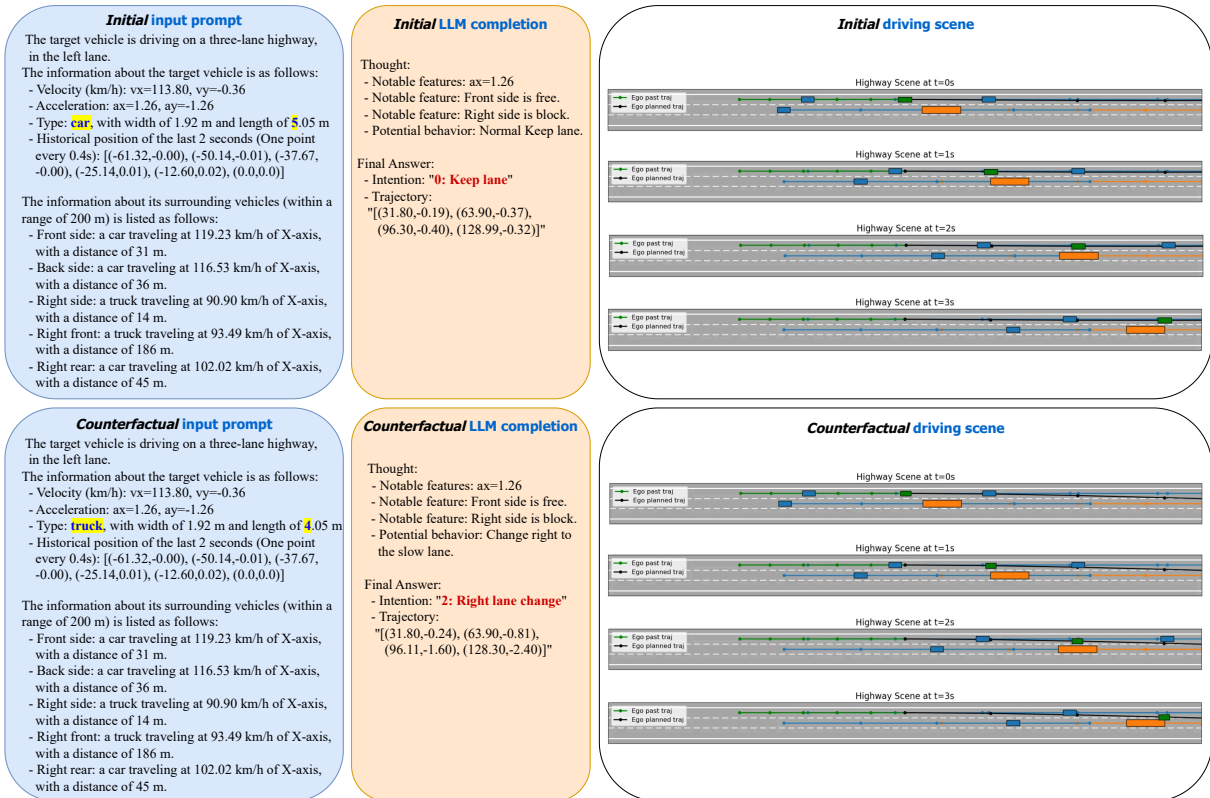


Figure 14: Visualization of a counterfactual explanation to explain the decision boundary of our 'vehicle' biased LLM, generated by DRIV-EX. In bold blue, we highlight characters that differ between the initial input and its counterfactual. The counterfactual driving scene shows that the planned trajectory leads to a collision at t=3 secs.

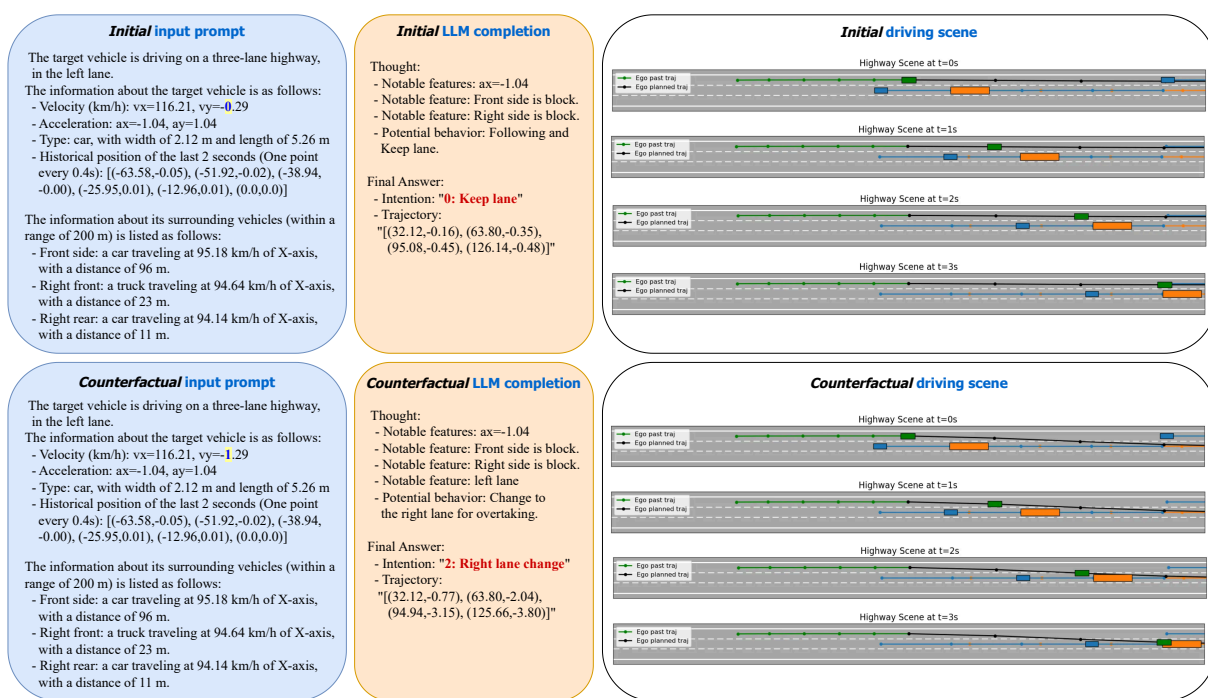


Figure 15: **Visualization of a counterfactual explanation revealing the ‘vy’ bias**, generated by DRIV-EX. In bold blue, we highlight characters that differ between the initial input and its counterfactual. The counterfactual driving scene shows that the planned trajectory leads to a collision at $t=3$ secs.